ACADEMIC PRESS

Available online at www.sciencedirect.com
SCIENCE DIRECT®

Journal of Catalysis 217 (2003) 354–366

JOURNAL OF CATALYSIS

www.elsevier.com/locate/jcat

Adsorption of unsaturated aldehydes on the (111) surface of a Pt–Fe alloy catalyst from first principles

Robin Hirschl,[a,b,c,*] Françoise Delbecq,[a,b] Philippe Sautet,[a,b] and Jürgen Hafner[c]

[a] *Institut de Recherches sur la Catalyse, CNRS, 2 Avenue Albert Einstein, F-69626 Villeurbanne cedex, France*
[b] *Laboratoire de Chimie, CNRS, École Normale Supérieure de Lyon, 46 Allée d'Italie, F-69364 Lyon cedex 07, France*
[c] *Institut für Materialphysik and Center for Computational Materials Science, Universität Wien, Sensengasse 8/12, A-1090 Wien, Austria*

Received 30 October 2002; revised 28 January 2003; accepted 3 February 2003

Abstract

Platinum surfaces alloyed with an electropositive metal (e.g., Fe, Sn) are known to largely improve the selectivity in the hydrogenation of α,β-unsaturated aldehydes toward unsaturated alcohols. We have investigated various adsorption modes for acrolein and prenal on the $Pt_{80}Fe_{20}$ (111) surface applying spin-polarized density-functional theory, following a similar recent study on a pure Pt (111) surface (F. Delbecq, P. Sautet, J. Catal. 211 (2002) 398). It turns out that only the existence of iron atoms in the surface layer bears the potential to influence the hydrogenation selectivity in favor of unsaturated alcohols. On the clean alloy surface there is a strong segregation of Pt atoms toward the surface layer, but a significantly higher aldehyde-adsorption energy upon the formation of O–Fe bonds can change the surface segregation profile, increasing the Fe content in the surface layer. The electronic structure changes due to O–Fe instead of O–Pt interactions will be discussed. Eventually, calculated vibrational spectra are presented as a link to experiments.

Keywords: Unsaturated aldehydes; Platinum; Iron; Alloy surface; Adsorption; Density functional theory

1. Introduction

Product selectivity and yield in heterogeneous catalytic reactions are significantly influenced by the nature of the catalyst employed. The selective hydrogenation of α,β-unsaturated aldehydes to unsaturated (allylic) alcohols has recently attracted much interest and the understanding of the origin of selectivity raises a great challenge to catalysis research in view of the complexity of the reaction [1–3]. Unsaturated alcohols, such as allyl alcohol (CH_2=CH–CH_2–OH), crotyl alcohol (CH_3–CH=CH–CH_2–OH), or 3-methylbutenol ((CH_3)$_2$–CH=CH–CH_2–OH), are important intermediates in fine chemistry, particularly in pharmaceuticals and cosmetics. Considering the low scale of production in these industries, high product yields and selectivity are often crucial. Hence, the realization of even a small increase in selectivity for the desired product would result in a large added value.

α,β-unsaturated aldehydes present two adjacent double bonds in conjugation, C=C and C=O. The simplest of these aldehydes are sketched in Fig. 1. The selective hydrogenation of only the C=O double bond is difficult to achieve because of two reasons [4,5]: (a) thermodynamics favors the hydrogenation of the C=C over the C=O group and (b) for kinetic reasons the reactivity of the C=C group in hydrogenation is supposed to be higher than that of the C=O group. Consequently, on conventional hydrogenation catalysts (Pt, Ru, Ni, etc.) the predominant products are either the saturated aldehydes (undesired because they can be produced by alkene hydroformylation in industrial chemistry) or the saturated alcohols from the consecutive hydrogenation of both double bonds.

The intramolecular selectivity in the hydrogenation of α,β-unsaturated aldehydes is controlled by various factors. Among others the selectivity to the unsaturated alcohols is generally increased by: (a) larger substituents on the terminal carbon atom of the C=C bond (C3); the substituents prevent the adsorption via this functional group and subsequent hydrogenation by Pauli repulsion; (b) using larger metal clusters when performing the reactions on nanoparticles because

* Corresponding author.
E-mail address: robin.hirschl@univie.ac.at (R. Hirschl).

0021-9517/03/$ – see front matter
doi:10.1016/S0021-9517(03)00057-5

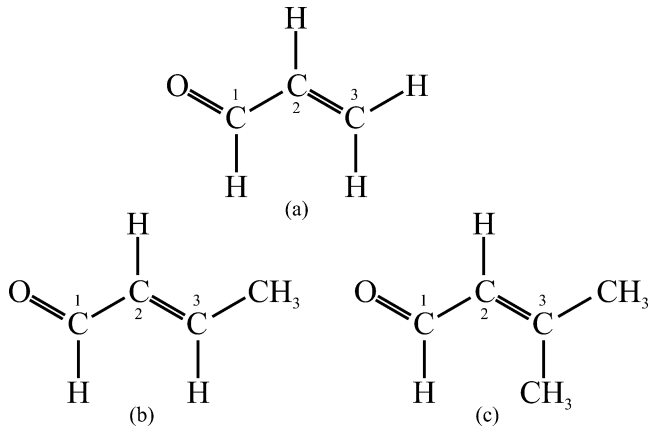

Fig. 1. Simple α,β-unsaturated aldehydes: (a) acrolein (2-propenal), (b) crotonaldehyde (2-butenal), and (c) prenal (3-methyl-2-butenal). The corresponding unsaturated alcohols are allyl alcohol, crotyl alcohol, and 3-methylbutenol, respectively. C atoms are numbered consecutively, starting from the one nearest to the oxygen.

Table 1
Experimentally determined selectivities for the hydrogenation of α,β-unsaturated aldehydes on well defined $Pt_{80}Fe_{20}$ surfaces and small $Pt_{0.8}Fe_{0.2}$ particles to the saturated aldehyde (SAL), the unsaturated alcohol (UOL), and the saturated alcohol (SOL)

	Pt			$Pt_{80}Fe_{20}$		
	SAL	UOL	SOL	SAL	UOL	SOL
Well-defined $Pt_{80}Fe_{20}$ (111) surfaces, Ref. [6]						
Crotonaldehyde		10			13	
Prenal		56			70	
Small $Pt_{0.8}Fe_{0.2}$ particles, Ref. [8]						
Acrolein	92.6	1.6	1.8	84.9	7.3	7.4
Crotonaldehyde	50.0	13.0	33.6	44.9	27.8	26.1
Prenal	17.0	20.5	55.0	5.1	80.4	14.4

of steric constraints on the metal surface; (c) electronic and steric effects due to ligands and supports (e.g., zeolites); (d) by modifying monometallic catalysts via addition of a second metal [2,6–9]. This second metal can either be an electropositive p-electron (e.g., Sn) or d-electron element (e.g., Fe).

We have investigated the capabilities of two simple α,β-unsaturated aldehydes (acrolein and prenal, Figs. 1a and c) to adsorb on the $Pt_{80}Fe_{20}$ (111) transition-metal-alloy surface. Experimentally determined selectivities of this alloy to the different possible reaction products are compiled in Table 1. It can be assumed that only intramolecular bonds, that are previously weakened through direct interaction of the constituting adsorbate atoms with the surface, might become activated for hydrogenation. Hence the relative strength of the various adsorption modes is of crucial interest. The results we present in the following, obtained from calculations based on local spin-density-functional theory [10,11], tie in with two recently published articles: On the one hand, we have investigated the local properties of $Pt_{80}Fe_{20}$ (111) surfaces using small probe adsorbates [12], on the other hand two of us (Delbecq and Sautet) have studied the adsorption of unsaturated aldehydes on pure Pt (111) surfaces [13]. Compared to the latter study, the present system posed an even larger calculational challenge because of the need of a spin-resolved treatment of the surface [12].

This paper is organized as follows: in Section 2 we describe the main points of our calculations and present a quasi-chemical model to investigate the segregation profile of the alloy surface. Section 3 introduces details of our surface models and discusses adsorption energies and geometries of the aldehydes. The formation of very strong O–Fe bonds might change the segregation profile of the alloy surface, an issue that is treated in Section 4. In Section 5 we briefly discuss some properties of the local electronic structure of both surface and adsorbate upon adsorption. Vibrational spectra present a means to connect our results to experimental investigations. The spectra of aldehydes adsorbed in different configurations are discussed in Section 6. Finally, Section 7 summarizes our results.

2. Methodology

2.1. DFT calculations

All calculations of ground-state energies and ionic relaxations have been performed in the framework of local spin-density-functional theory by the use of the plane-wave-based Vienna ab initio simulation package (VASP) [14,15] to solve the single-particle Kohn–Sham equations. The local density approximation for the exchange-correlation functional was improved by using the generalized gradient approximation (GGA) as proposed by Perdew and Wang (PW91) [16]. Brillouin-zone sampling was performed on Monkhorst–Pack special points [17], integrated utilizing a generalized Gaussian smearing. The plane-wave cutoff was set to 400 eV throughout all calculations, the k-point mesh was chosen to $(6\times6\times1)$ and $(3\times3\times1)$ k-points in (2×2) and $(2\sqrt{3}\times2\sqrt{3})$ supercells. Sufficient convergence with respect to energy cutoff and number of k-points was confirmed.

The projector-augmented-wave (PAW) method of Blöchl [18], in the formulation of Kresse and Joubert [19], is applied to describe electron–ion interactions. This method, being essentially all electron, improves the description of transition metals compared to the use of pseudopotentials. 3p states of iron are treated as valence states to guarantee a good transferability of the potential.

Plane-wave-based codes necessitate periodic boundary conditions, which in turn fix a slab geometry as the setup of choice. Our supercell consisted of 4 layers of substrate, separated by 4 to 7 layers of vacuum, depending on the adsorption mode. Vertically adsorbed aldehydes possess a large dipole moment. Not only does the periodic lattice of dipoles introduce errors, but also the dipoles cause spurious charges in the surface [20]. These effects considerably slow down the

energy convergence with respect to the size L of the supercell. They can be counterbalanced by adding a linear electrostatic potential to the local potential [21]. However, the automatically determined corrections adversely influence the convergence of the wavefunctions in the iterative solution of the Kohn–Sham equations. The importance of dipole corrections for upright adsorption modes will be discussed below. Ionic relaxation of the adsorbate and of the topmost surface layers is performed after determining the Hellmann–Feynman forces [22] acting on the atoms.

The full vibrational spectrum of a molecule or an adsorbate can be obtained by numerically approximating the Hessian matrix using finite differences and evaluating its eigenvalues. In the case of adsorbates this approach neglects the coupling of the adsorbate vibrations to the surface phonons, which luckily introduces significant errors only for the lowest adsorbate frequencies. For adsorbate frequencies corresponding to the stretching vibrations of individual bonds, which are generally orders of magnitude higher than surface phonon frequencies, the omission of adsorbate-surface coupling is certainly reasonable. The correct determination of vibrational frequencies requires mainly the accurate description of the ionic ground state. Since we compare systems that differ only by a tiny shift of certain atoms, DFT-specific systematic errors have only little influence on the frequencies.

2.2. Segregation profile

Atoms near the surface of an (alloy) crystal are subjected to forces other than those residing in the bulk. This leads in many cases to surface segregation, relaxation, reconstruction, and (dis)ordering processes [23]. As these changes may have a substantial impact on the chemical reactivity of the alloy surface, a detailed knowledge of the composition and geometry of the surface under catalytic conditions is highly desirable. Following Creemers [24] and Creemers and Deurinck [25], we will introduce a simple quasi-chemical model to qualitatively determine the composition of the topmost surface layer in a $Pt_{80}Fe_{20}$ (111) alloy surface under the influence of adsorbates.

Segregation occurs spontaneously because the alloy can, by reordering of the atoms, lower its Gibbs free energy in a surrounding at a given temperature and pressure. The equilibrium surface composition corresponds to the situation of minimal Gibbs energy. In the following we consider only the top two layers of the alloy surface, initially consisting of 80 at% Pt and 20 at% Fe with no Fe–Fe nearest neighbors. It is known from experiment that the topmost layer of the clean surface almost entirely consists of platinum. Consequently, in the simplest model the only process allowed to contribute to surface segregation is the interchange of surface Fe atoms with underlying Pt nearest neighbors, treated as a chemical reaction,

$$\mathrm{Fe}_{\mathrm{Fe},1} + \mathrm{Pt}_{\mathrm{Pt},2} \overset{\Delta}{\rightleftharpoons} \mathrm{Pt}_{\mathrm{Fe},1} + \mathrm{Fe}_{\mathrm{Pt},2}. \tag{1}$$

The subscripts denote Fe and Pt sites in the surface (1) and subsurface (2) layers, respectively. Reaction (1) describes the exchange at equilibrium of Δ at% second-layer Pt atoms with first-layer Fe atoms. The allowed surface-layer platinum content in our model is therefore 80 at% $\leqslant x_{\mathrm{Pt},1} \leqslant$ 100 at%. The associated equilibrium equation,

$$RT \ln K_{\mathrm{seg}} + \Delta G^0_{\mathrm{seg}} = 0, \tag{2}$$

has two unknown terms, the equilibrium constant, K_{seg}, and the excess Gibbs energy for segregation, $\Delta G^0_{\mathrm{seg}}$. Calculating the configurational entropy through Boltzmann's well-known equation $S = k_{\mathrm{B}} \ln W$, W being the number of microscopic permutations yielding the same macroscopic concentration, one obtains for the rate constant [25]

$$K_{\mathrm{seg}} = \frac{\Delta}{3(0.2 - \Delta)}. \tag{3}$$

The excess Gibbs energy is determined from a constant bond-energy assumption, including the change in surface energy, the change in total bond energy, and a possible "chemical pump effect" [26] due to a preferential chemisorption of an external species on different surface species (ΔE_{ad}). Since the resulting $\Delta G^0_{\mathrm{seg}}$ contains the equilibrium Pt-concentration change Δ as well as the rate constant K_{seg}, Eq. (2) eventually has to be solved numerically.

It shall be noted again that this crude model is only qualitative. Nevertheless, it provides important insights in the alloy-surface composition as will be discussed in Section 4, avoiding at the same time the implementation of time-consuming more sophisticated algorithms that are not expected to substantially change the picture.

3. Adsorption geometries and energies

3.1. Surface model

Following experimental investigations of the $Pt_{80}Fe_{20}$ (111) surface [25,27,28], the initial model consists of a Pt_3Fe bulk terminated by a single layer of pure Pt (cf. Fig. 2 and our previous discussion in [12]). The model leads to two geometrically inequivalent Pt sites in the surface, distinguished by the existence or non existence of a subsurface Fe nearest neighbor, labeled Pt1 and Pt2, respectively. The calculated supercell consists of 4 layers of 12 atoms each, layers below the surface contain 3 Fe atoms per supercell. To test the influence of Fe atoms in the surface, one of the subsurface iron atoms was interchanged with a surface Pt nearest neighbor (see insets in Fig 2). This surface is henceforth referred to as "modified $Pt_{80}Fe_{20}$" surface. Details regarding the surface relaxation and electronic structure can be found in [12].

3.2. Adsorption energies

Theoretical investigations on the stability of different adsorption modes of unsaturated aldehydes on pure Pt (111)

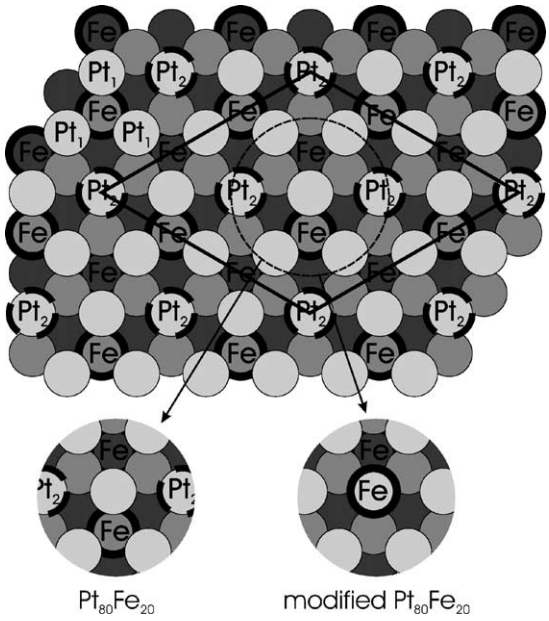

Fig. 2. Model of the $Pt_{80}Fe_{20}$ (111) surface used for calculations. The $(2\sqrt{3} \times 2\sqrt{3})R30°$ supercell is marked by the thick line. The surface has two types of Pt atoms in the surface layer (cf. main text). In the modified $Pt_{80}Fe_{20}$ (111) surface one Pt atom of type 1 per supercell is interchanged with an underlying Fe atom.

surfaces have been published lately [13], including many references to experimental works on that system. Calculations on the reactivity of alloy systems began only recently because of previous lack of computational resources. One of the very few earlier works, generally employing semiempirical methods, is our (Delbecq and Sautet) extended Hückel study of acrolein and crotonaldehyde on $Pt_{80}Fe_{20}$ surfaces, which initiated the present much broader and more detailed approach. More recent theoretical works on the chemical reactivity of PtM alloy surfaces include the adsorption of ethylene and oxygen on Pt_3Sn (111) by Watwe et al. [29] and the adsorption of ethylene and formaldehyde on Pt_3Zn (111) by Silvestre-Albero and co-workers [30].

Experimental studies regarding the influence of electropositive additions to platinum surfaces on their catalytic abilities to selectively hydrogenate a certain double bond have begun much earlier. In this context the investigation of $Pt_{80}Fe_{20}$ (111) surfaces was pioneered by Beccat et al. in 1990 [6]. Still, this class of systems has not lost any of its fascination since, as recent publications prove—see, e.g., the investigation of vapor-phase hydrogenation of crotonaldehyde over magnesia-supported platinum–tin catalysts by Homs et al. [9]. The adsorption of acrolein and crotonaldehyde on pure Pt (111) surfaces was experimentally investigated among others by de Jesús and Zaera [31] using reflection-absorption infrared spectroscopies (RAIRS). Bailie et al. [32] studied the hydrogenation of acrolein over Co/SiO_2 and Co_3O_4/SiO_2 via vibrational spectra. They concluded that on their surfaces C=O bonds are only hydrogenated through Co^{n+} sites, either on the oxide or through reduction of the metal surface. These cations have a large affinity for the O atoms of the aldehydes. A slightly different approach to the selective hydrogenation of unsaturated aldehydes toward unsaturated alcohols has recently gained attention, namely the use of noble-metal nanoclusters, particularly gold [5,33].

Coming to the different adsorption structures of α,β-unsaturated aldehydes on surfaces, there are various possibilities, since each of the two double bonds can interact, separately or in combination, with the metal atoms. A double bond can interact with the substrate in two different ways, either the atoms at both ends of the bond interact with different atoms in the surface (diσ configuration), or the π-electrons of the double bond interact with a single surface atom (π adsorption). Furthermore, there are *cis*- and *trans*-configurations of the aldehydes, depending on the relative position of the terminating oxygen and the C3 atom, increasing the number of possible adsorption modes. The structures can be divided into four classes: interaction with the substrate via the C=C bond, the C=O bond, both bonds simultaneously (this configuration is referred to as η_4, following the conventions in organometallic chemistry), and via the oxygen lone pair. The last class of configurations leads to an upright configuration of the adsorbate, while all other adsorption modes are more or less flat. Two other configurations have been considered: a diσ_{CC} mode with additionally the oxygen atom interacting with the surface (labeled η_3) and a ring-shaped adsorption mode with the oxygen and the C3 atom interacting with neighboring metal atoms, leading to an organometallic ring, termed diσ-14 mode. A representative example for every class is depicted in Fig. 3.

The existence of two types of Pt surface atoms in the alloy surface again multiplies the number of inequivalent adsorption modes. Considering π and diσ modes for the interactions via a single double bond this would add up to more than 40 different configurations for a single adsorbate, a number unacceptable regarding computational demand. For the choice of the geometries eventually tested we established three criteria: (a) every class of adsorption modes should be considered at least once for the simplest unsaturated aldehyde, acrolein, on the alloy surface (however, judging from previous results on ethylene [30] and formaldehyde [34], adsorption through a single π-interaction can be discarded), (b) particularly concerning *cis–trans* selection we chose the structure more stable on the pure Pt surface [13], (c) results for acrolein qualified the choices for the more complex adsorbate prenal.

The adsorption energies per atom as well as per surface area are collected in Table 2. A few configurations on pure Pt (111) were considered to compare the results with the ones in [13], where a slightly different calculational setup (e.g., ultrasoft (US) instead of PAW potentials) was used. Adsorption energies agree accurately, as close as 10 meV for the η_4 prenal adsorption mode (1 kcal/mol $\equiv$ 43.393 meV/molecule). On the pure Pt (111) surface the diσ_{CC} adsorption mode is by far more stable than the adsorption via the C=O double bond. However, adsorption

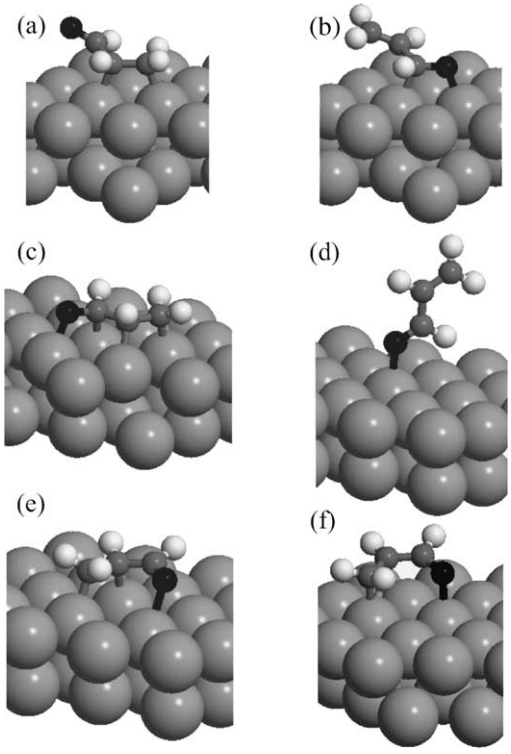

Fig. 3. Adsorption modes for α,β-unsaturated aldehydes on metal surfaces: diσ_{CC} (a), diσ_{CO} (b), η_4-*trans* (c), top (d), η_3-*cis* (e), diσ-14 (f). The adsorbate in the drawings is acrolein, the simplest of this class of aldehydes.

via bouth double bonds (η_4-*trans*) is, at least at $T = 0$ K and low coverages ($\Theta = 1/12$), the most stable configuration. At higher coverages ($\Theta = 1/4$), configurations with fewer adsorbate-surface interactions are prevalent [13]. Both aldehydes (acrolein and prenal) show the same energetical ordering of configurations, although the difference between diσ_{CC} and diσ_{CO} is reduced for prenal. Furthermore, the top adsorption mode becomes competitive on the pure platinum surface as the size of the substituents on the C3 atom increases [13].

Turning now to the platinum-covered alloy surface we observe an overall reduction of adsorption energies, similar to our previous findings for the adsorption of CO and atomic hydrogen on that surface [12]. From the diσ energies it can be clearly seen that the Pt2 atoms, being less influenced by iron atoms, bind stronger to carbon atoms, while this is not the case for oxygen atoms of the adsorbate. For other adsorption modes than diσ_{CC} and diσ_{CO} we have consequently preferred Pt2–C interactions. The adsorption via the C=O double bond is barely stable. Furthermore, η_3-*cis* becomes the most favorable adsorption geometry, 0.140 eV more stable than η_4-*trans*, which is the favored adsorption mode on pure Pt for this coverage. Adsorption via the formation of an organometallic ring (diσ-14) is not competitive.

Vertical adsorption (top mode) is allowed for a coverage up to a quarter monolayer. Nevertheless the adsorption

Table 2
Adsorption energies of acrolein and prenal per adsorbate and per surface area for selected adsorption modes and different surfaces (see main text for a justification of the choices)

Configuration	Adsorbate–surface interaction	Coverage	E_{ad} acrolein		E_{ad} prenal	
			(eV/molecule)	(meV/Å^2)	(eV/molecule)	(meV/Å^2)
Pt (111)						
diσ_{CC}	C_2–Pt, C_3–Pt	1/12	1.042	30.85		
diσ_{CO}	O–Pt, C_1–Pt	1/12	0.248	7.34		
η_4-*trans*	O–Pt_1, C_1–Pt_1, C_2–Pt_2, C_3–Pt_1	1/12	1.134	33.56	0.671	19.86
$Pt_{80}Fe_{20}$ (111)						
diσ_{CC}	C_2–Pt_1, C_3–Pt_1	1/12	0.584	17.64		
diσ_{CC}	C_2–Pt_2, C_3–Pt_1	1/12	0.722	21.81		
diσ_{CC}	C_2–Pt_1, C_3–Pt_2	1/12	0.727	21.97	0.321	9.70
diσ_{CO}	O–Pt_1, C_1–Pt_1	1/12	0.004	0.12		
diσ_{CO}	O–Pt_2, C_1–Pt_1	1/12	−0.053	−1.60	−0.077	−2.33
diσ_{CO}	O–Pt_1, C_1–Pt_2	1/12	0.084	2.54	0.068	2.05
η_3-*cis*	O–Pt_1, C_2–Pt_2, C_3–Pt_1	1/12	0.768	23.20	0.155	4.68
η_4-*cis*	O–Pt_1,C_1–Pt_1, C_{23}–Pt_2	1/12	0.591	17.86	0.305	9.21
η_4-*trans*	O–Pt_1, C_1–Pt_1, C_2–Pt_2, C_3–Pt_1	1/12	0.628	18.97	0.180	5.44
diσ-14	O–Pt_1, C_3–Pt_2	1/12	0.425	12.84		
top	O–Pt_2	1/12	0.126	3.81		
top	O–Pt_2	1/4	0.010	0.91	0.032	2.90
Mod. $Pt_{80}Fe_{20}$ (111)						
diσ_{CC}	C_2–Pt, C_3–Fe	1/12	0.482	14.56		
diσ_{CO}	O–Fe, C_1–Pt	1/12	0.681	20.58	0.688	20.78
η_3-*cis*	O–Fe, C_1–Pt, C_2–Pt	1/12	1.476	44.59	0.971	29.33
η_4-*trans*	O–Fe_1, C_1–Pt_1, C_2–Pt_2, C_3–Pt_1	1/12	1.247	37.67	0.788	23.80
diσ-14	O–Fe, C_3–Pt	1/12	1.090	32.93	0.679	20.51
top	O–Fe	1/12	0.558	16.86	0.383	11.57
top	O–Fe	1/4	0.493	44.69	0.474	42.95

Adsorbate–surface interactions are listed in the second column. All adsorption energies are given without dipole corrections, cf. main text for details.

energy is far from that of flat adsorption configurations. The energies given in Table 2 are calculated without dipole corrections (cf. Section 2), which decrease the energies further by 60–70 meV compared to our initial setup with 6 layers of vacuum separating the slabs, disfavoring the vertical adsorption modes even more compared to the flat ones.

For prenal the adsorption via the C=C double bond is weaker than for acrolein due to the two methyl groups on the C3 atom. They do not, however, influence the adsorption via the C=O bond, bringing the adsorption energy difference between the two diσ configurations down to 0.253 eV. Also, other adsorption geometries involving a diσ interaction of the C=C bond with the surface (η_3-*cis* and η_4-*trans*) are drastically destabilized compared to acrolein. Nevertheless, an η_4-*cis* configuration, including a π interaction of the C=C double bond with a Pt2 surface atom, is energetically close to the most favorable configuration, diσ_{CC}.

Eventually we tested the influence of an Fe atom brought up to the surface layer of the alloy surface (cf. Fig. 2 and last part of Table 2), having a large affinity for the oxygen atom in the molecule. Adsorption energies for configurations with no interaction of the surface iron atom with the adsorbate are expected to be similar to the adsorption on the platinum-covered alloy surface. The formation of very strong Fe–O bonds shifts the adsorption energies in favor of geometries including the interaction of the oxygen atom with the surface. For acrolein, diσ_{CO} is 0.2 eV more stable than diσ_{CC}, with one atom of the C=C double bond bound to the Fe surface atom and only slightly less stable (0.05 eV) than the best diσ_{CC} configuration on the platinum covered alloy surface. η_4-*trans* and η_3-*cis* become by far the most stable configurations, more stable than any other configuration, including the pure Pt (111) surface. The same is true for prenal, clearing the way for a hydrogenation of the C=O double bond, which is exposed to the attack of coadsorbed hydrogen.

Also a vertical adsorption geometry becomes very competitive because of the possible high coverage. We note that for prenal even the adsorption energy per molecule increases with coverage, because at $1/4$ coverage the hydrogen atoms of neighboring adsorbates approach each other as close as 2 Å, leading to stabilizing dipole–dipole interactions as was confirmed by calculating high densities of prenal in vacuum. Adding again dipole corrections to the values in Table 2 reduces the energies by about 70 meV or 6.3 meV/Å^2 for a coverage of $\Theta = 1/4$. Still this mode remains the most favorable configuration regarding the adsorption energy per area. However, for the preferred adsorption mode at catalytic conditions (ambient temperature), entropic effects must be taken into account. The entropy of the adsorbed molecules must be compared with the entropy in the liquid (or gas) phase. A quantitative estimation is difficult since data on the entropy of prenal in the liquid phase are rare. An approximate model using the entropy of similar molecules leads to the conclusion that at normal pressure the transition temperature from top to η_3-*cis* adsorption is well below 100 K, letting us assume a flat adsorption geometry under catalytic conditions.

3.3. Adsorption geometries

Characteristic bond lengths for prenal in the gas phase and adsorbed in several configurations on platinum-covered and modified $Pt_{80}Fe_{20}$ surfaces are given in Fig. 4 and Table 3. Upon adsorption the lengths of the bonds interacting with the surface are elongated and intermolecular angles are changed. The latter originates in a transformation from a planar sp^2-like hybridization of the carbon orbitals to a tetrahedral sp^3-like hybridization, with bond angles in the

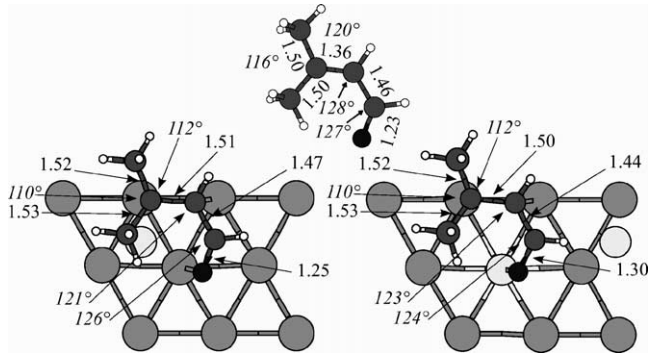

Fig. 4. Intermolecular bond lengths and angles for gaseous *cis*-prenal (top), prenal η_3-*cis* adsorbed on platinum-covered $Pt_{80}Fe_{20}$ (bottom left), and the same adsorption mode on modified $Pt_{80}Fe_{20}$ (bottom right). Only surface-layer atoms and second-layer iron atoms are drawn (iron represented by the bright circles). All distances are in Å. The influence of the Fe surface atom is clearly reflected in the geometry of the adsorbate.

Table 3
Intermolecular and metal–adsorbate bond lengths for prenal adsorbed on a platinum-covered and on a modified $Pt_{80}Fe_{20}$ alloy surface

Mode	Surface	E_{ad} (eV)	O–C_1	C_1–C_2	C_2–C_3	O–surface	C_1–surface	C_2–surface	C_3–surface
Gas		–	1.23	1.46	1.36				
diσ_{CC}	PtFe	0.359	1.23	1.49	1.51			2.17	2.16
diσ_{CO}	PtFe	0.106	1.34	1.45	1.36	2.11	2.24		
η_3	PtFe	0.193	1.25	1.47	1.51	2.46	2.73	2.18	2.16
η_4-*trans*	PtFe	0.218	1.31	1.49	1.50	2.16	2.31	2.15	2.18
η_3	Modified	1.009	1.30	1.44	1.50	2.01	2.47	2.20	2.14
η_4-*trans*	Modified	0.826	1.35	1.50	1.50	1.90	2.14	2.17	2.18
Top	Modified	0.474	1.26	1.44	1.36	2.16			

All distances in Å. For comparison the bond lengths in the gas phase are given.

case of full hybridization of 120 and 109.5°, respectively. The resulting decrease of bond angles in the prenal molecule is most pronounced around the C3 atom with the two attached methyl groups.

Regarding bond lengths, the primary indication for the weakening of a bond is the increase of its length compared to the gas phase. Comparing the two diσ adsorption geometries with the free molecule, we observe an increase in the length of the bond interacting with the substrate by about 10%, similar to the results on a pure Pt (111) surface [13]. We further note that whenever the C=C double bond interacts with the surface in a diσ configuration, the bond length is equally increased. Comparing this to the bond-length increase of the C=O double bond upon adsorption, an elongation as large as 10% only occurs for the diσ_{CO} mode on the platinum-covered surface and the η_4-*trans* mode on the modified surface. In the η_3 adsorption modes the C=O double bond mainly interacts with the surface via the lone pair of the oxygen atom. This orbital is not a bonding C=O orbital, leading to an only moderate increase in the bond length. Metal–oxygen bond lengths in organometallic complexes are usually around 2 Å [35,36]. The Pt–O bond in the η_3-*cis* adsorption, being 2.46 Å, is considerably larger than that, showing a weak interaction. In contrast, the Fe–O bond length for all listed adsorbate configurations on the modified alloy surface is $\approx$ 2 Å, indicating the formation of a metal–oxygen bond with a strength comparable to that in organometallic complexes.

Combining all information about adsorption energies and bond length changes on different surfaces we can establish a correlation between the adsorption energy and the weakening of the double bonds as expressed by the increase in their lengths. It is expected that the barrier for hydrogenation of a double bond is the lower the weaker the bond, and consequently the C=O bond hydrogenation will be easier upon aldehyde adsorption on the modified alloy surface.

4. Alloy surface segregation profile

The quasi-chemical model we have used to describe the segregation in the top layer of the $Pt_{80}Fe_{20}$ surface has been outlined in Section 2.2. It has been used in the context of the alloy surface discussed here before [25], correctly describing the strong Pt segregation toward the surface, without any consideration of adsorption energies. Input parameters for the model are the bond energies of the individual metals and the regular solution parameter, which is calculated from the heat of mixing. While those parameters previously were derived from experimental values for the heats of sublimation and the heat of mixing for the 50–50% alloy, we have determined them from ab initio calculations. The heat of mixing was taken from the ordered Pt_3Fe alloy, since this is the underlying superstructure that is modified by segregation. A simple example justifies the use of our crude model for the qualitative analysis of the segregation: Counting all bonds when changing from the initial to the modified $Pt_{80}Fe_{20}$ surface yields an increase of 3 Pt–Pt bonds at the cost of Pt–Fe bonds. The corresponding change in total energy assuming constant bond energies is 0.75 eV, in remarkably good agreement with the calculated energy difference of 0.85 eV.

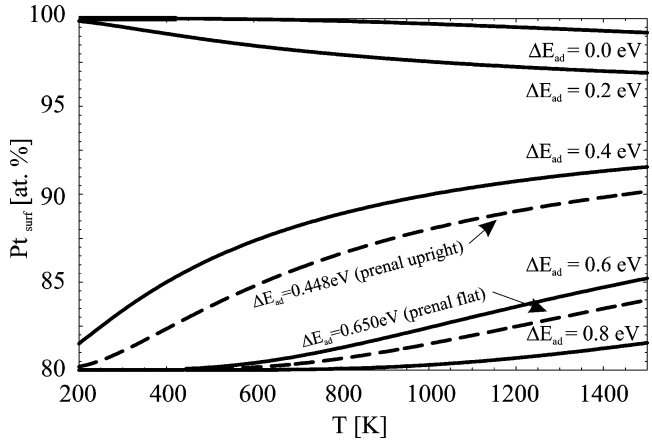

Fig. 5. Adsorption-induced change of the segregation calculated in a simple quasi-chemical model for the interchange of surface Fe with subsurface Fe atoms in $Pt_{80}Fe_{20}$ (111) and assuming different values for the difference in the molecular adsorption energies on Fe or Pt atoms ΔE_{ad}. The dashed lines use the adsorption energy differences determined for flat and upright prenal with/without iron atoms in the surface layer.

Surfaces similar to $Pt_{80}Fe_{20}$ studied theoretically for surface segregation are $Fe_{99}Pd_1$ [24] and Pd–X alloys (X = Pt, Ag, Au, Cu) [37]. In the former alloy, an enrichment of Pd in the surface layer up to 55% was found. However, both studies do not include the effect of adsorbates on the segregation profile. Khanra and co-workers have studied the effect of sulfur on the composition profile of Pt–Rh nanocatalysts [38], and the spatial distribution of atoms in gas-covered Pd–X nanoparticles [39]. To note just one of their results: In $Pd_{50}Ni_{50}$ alloys the surface fraction of Pd atoms rises from 45 to 80 at% upon the adsorption of one monolayer of CO. The adsorption energy difference of CO adsorbed on Pd and Ni is 0.3 eV.

Adsorbate-induced segregation profile changes have also been investigated experimentally. Deckers et al. [40] have pioneered the determination of depth profiles using medium energy ion scattering (MEIS). They investigated the oxygen-induced segregation in the $Pt_{50}Ni_{50}$ (111) surfaces [41]. Only recently, Baddeley et al. [42] have studied adsorbate-induced segregation in $Cu_{50}Pd_{50}$ (110) surfaces. They found that hydrocarbon adsorption leads to Pd segregation, while the adsorption of atomic C or Cl leads to Cu segregation. The concentration of Cu in the first layer changes from 65 at% in the clean surface to 57 and 71 at% upon adsorption of ethylene and 1,2-dichlorethylene at 323 K, respectively, without further thermal treatment of the surface.

The results of our calculations are shown in Fig. 5. The model starts from a bulk-like distribution in every layer

(20 at% Fe) and allows for the interchange of a surface Fe atom with a neighboring subsurface Pt atom. The high temperature limit (complete disorder) is 95 at% Pt (one-quarter of the tetrahedra consisting of the surface atoms and the three underlying nearest neighbors has the Fe atom in the surface layer). In agreement with experiment, in the clean surface at room temperature the surface layer consists solely of platinum atoms.

When iron atoms are present in the surface layer, the unsaturated aldehydes bind significantly stronger to the surface than on a completely platinum-covered alloy surface. We observe from Fig. 5 that already at an adsorption energy difference around 350 meV with/without iron atoms in the surface, the surface layer Pt concentration at 200 K changes drastically from almost 100 at% to slightly above 80 at%. We recall that 80 at% is the minimum that our model allows; 350 meV is the energy needed for the interchange of a surface–platinum which a subsurface–iron atom in the constant bond-energy approximation. The calculated adsorption-energy differences are about 450 meV for vertically adsorbed and 650 meV for horizontally adsorbed prenal. This is well above the limit for which a considerable adsorption-induced segregation-profile change occurs. From the experimental evidence that an adsorption-induced segregation-profile change occurs already at room temperature in $Cu_{50}Pd_{50}$ (110) [42] and the results from our model calculations, we can conclude that iron atoms diffuse to the surface upon adsorption of unsaturated aldehydes under catalytic conditions (i.e., at ambient temperature (300 K) or slightly above), restoring an almost bulk-like composition of the surface.

5. Electronic structure

To our knowledge, an attempt to study the local electronic structure of such a complex system as unsaturated aldehydes adsorbed on transition-metal-alloy surfaces from first principles has not been made so far. In one of the first theoretical investigations of the $Pt_{80}Fe_{20}$ system two of us (Delbecq and Sautet) have discussed the orbital-resolved density of states of the clean surface and after the adsorption of atomic H, as obtained from semiempirical nonmagnetic extended Hückel calculations [43]. In a recent article we have presented spin-resolved DFT electronic structure data of the clean $Pt_{80}Fe_{20}$ (111) surface and its modification by test adsorbates [12]. In the present article, we will restrict ourselves to the analysis of the influence of surface iron atoms on the local electronic structure of the aldehyde/substrate complex.

We begin with the electronic structure of the subsurface and surface Fe atoms in $Pt_{80}Fe_{20}$ and modified $Pt_{80}Fe_{20}$ surfaces (Fig. 6). d-Band centers of mass (COM) are given in eV below E_{Fermi}. The slight deviations in the d-band COM of the Fe atoms in the platinum-covered surface with respect to the values given in Fig. 2b of [12] are a result of the different supercells used. Due to the lower coordination of

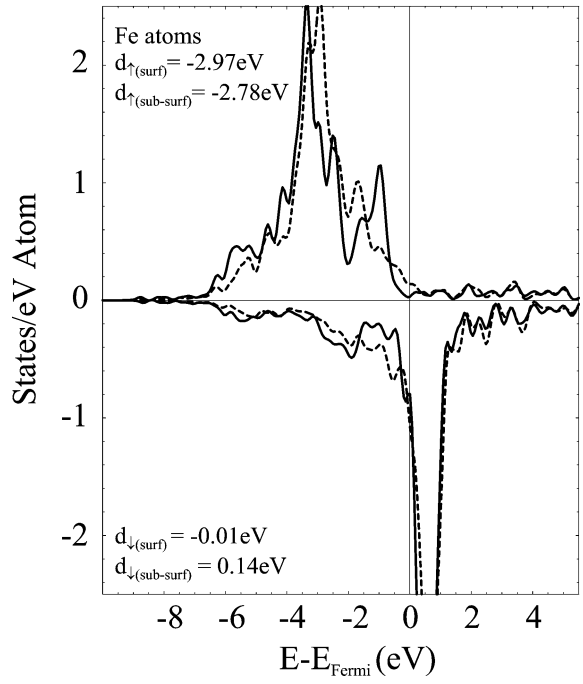

Fig. 6. Local density of states of subsurface iron atoms in platinum-covered $Pt_{80}Fe_{20}$ alloy surfaces (full lines) and surface iron atoms in modified $Pt_{80}Fe_{20}$ (cf. Fig. 2, dashed lines). d-Band centers of mass are given in eV below E_{Fermi}.

the iron atoms in the surface (only 9 Pt nearest neighbors instead of 12 in the subsurface layer), the main peak in the majority-spin component is less shifted toward higher binding energies. The majority-spin band of Fe is the one interacting most strongly with the Pt d-bands because of lying in the same energy range. Following the Hammer–Nørskov model [44], a d-band closer to E_{Fermi}, as is the case for surface relative to subsurface iron atoms, favors adsorbate/substrate interaction in two ways: On one hand the interaction of the "frontier" orbitals of the surface with unoccupied molecular orbitals of the adsorbate is increased because of the smaller energy difference, on the other hand antibonding states from four-electron interactions of filled substrate bands with filled molecular orbitals are more likely to be above E_{Fermi}, and hence unoccupied.

The two top panels (a,b) of Fig. 7 display the local densities of states of surface atoms interacting with the oxygen atom of prenal, compared to the respective electronic structures of the clean surface. The changes in the electronic densities of a platinum atom in the Pt-covered surface (Fig. 7a) after interaction with oxygen are rather moderate and not very telling. There is a slight shift of the d-band toward higher binding energies for η_3 adsorption, a second-order effect from neighboring Pt atoms which interact with the C=C double bond of the adsorbate. After a vertical adsorption of prenal the spin-up Pt d-band experiences a small shift toward lower binding energies due to the interaction with the low-lying oxygen p orbital, while the spin-down band is slightly shifted in the other direction. There is a loss of about 0.05 electrons in the Pt d-band for

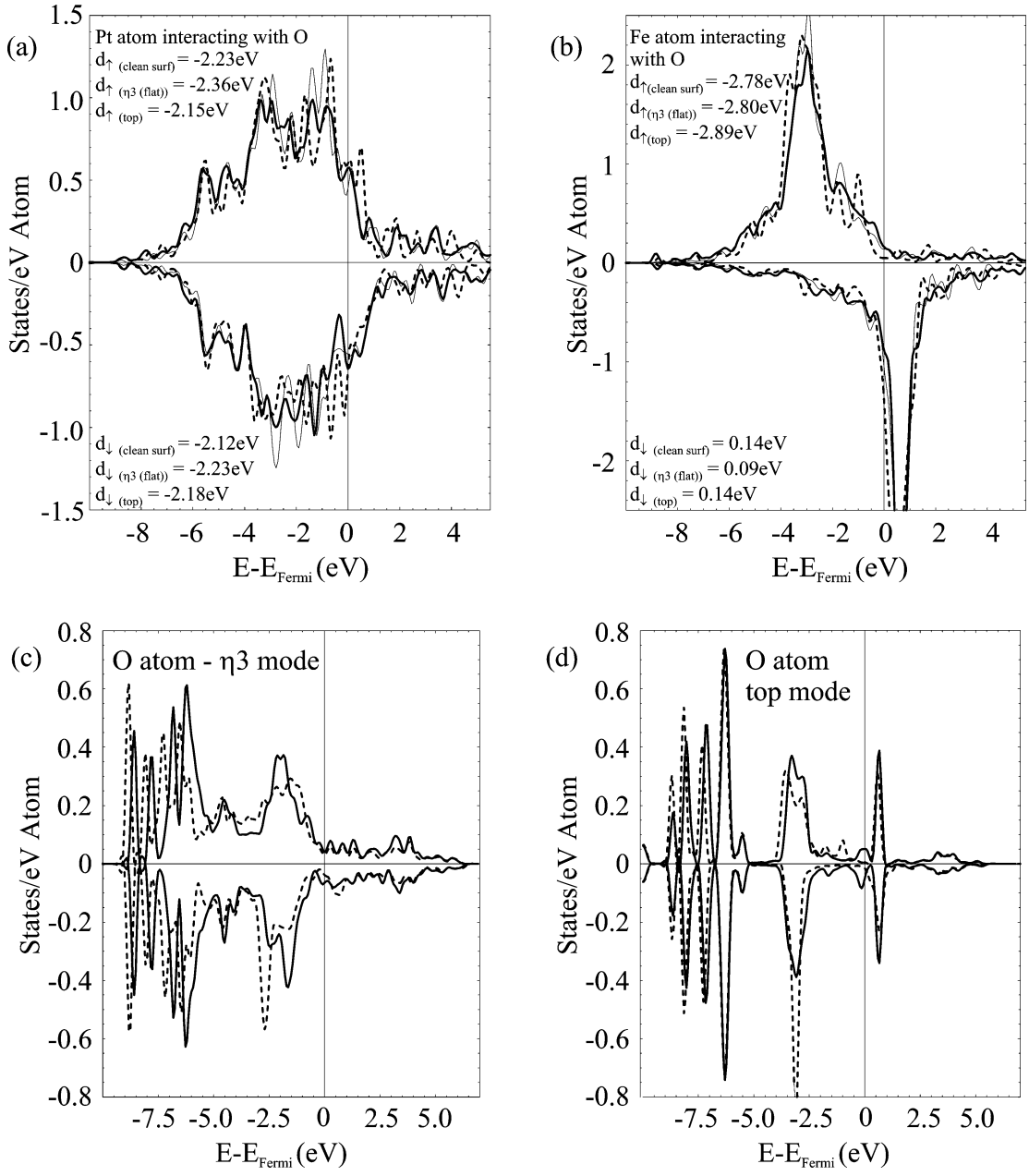

Fig. 7. LDOS of metal atoms interacting with an oxygen atom of prenal in flat (η_3, full lines) and upright (top, dashed lines) adsorption configurations: (a) Pt in $Pt_{80}Fe_{20}$, (b) Fe in modified $Pt_{80}Fe_{20}$ (the LDOS of the respective atoms in the clean surface are indicated by the thin lines); and LDOS of the oxygen atom in adsorbed prenal interacting with Pt (full line) and Fe (dashed line): (c) η_3 adsorption mode, (d) top adsorption mode. d-Band centers of mass are given in eV below E_{Fermi}.

vertical adsorption, but no change in the d-band occupation after η_3 adsorption.

The interaction of oxygen with iron atoms (Fig. 7b) is stronger, and again more pronounced for top adsorption than for the flat η_3 adsorption configuration. The main peak in the majority-spin band is lowered and broadened with respect to the clean surface the change in the electronic structure upon adsorption can easily be observed. While for η_3 adsorption electron donation by the substrate is again negligible, partly due to interferences with neighboring Pt atoms that also interact with the adsorbate, it is as large as 0.1 electrons for top adsorption. These electrons come from the minority-spin band, consequently the magnetic moment of the iron atom, being 3.22 μ_B in the clean surface and the η_3 configuration, rises slightly to 3.32 μ_B.

Panels c and d of Fig. 7 show the local densities of states of the oxygen atom in η_3-adsorbed (c) and top-adsorbed prenal (d), on platinum-covered $Pt_{80}Fe_{20}$ (full lines) and modified $Pt_{80}Fe_{20}$ (dashed lines). On comparing the two subfigures we note that the distinctive molecular-orbital peaks become more diluted for the flat than for the vertical adsorption configuration. This is not surprising

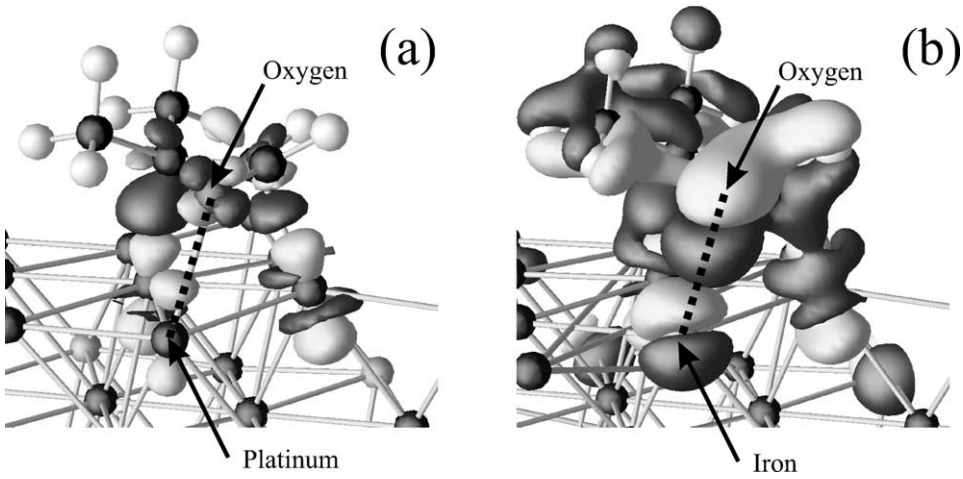

Fig. 8. Isosurface of the difference electron density of the prenal-metal system with respect to the sum of molecule and surface charge density for the η_3 adsorption mode on $Pt_{80}Fe_{20}$ (a) and modified $Pt_{80}Fe_{20}$ (b). Charge gain and loss are represented by dark and light shading, respectively. The same numerical values have been used for the respective isosurfaces of the two subfigures.

considering the more extended and considerably stronger adsorbate-metal interaction. In the η_3 configuration the whole delocalized π-system interacts with the surface by the contributions of the C2 and C3 atoms, contrary to the top configuration where the molecular π-system stays intact. In the latter case it remains as sharp peaks in the electronic density of states. We further note in both figures a pronounced peak in the spin-down band around 3 eV below E_{Fermi} when the oxygen atom interacts with a surface iron atom. The induced magnetic moment of oxygen remains in all cases below 0.04 μ_B.

In Fig. 8 we have plotted the charge flow when a prenal molecule adsorbs in the η_3 configuration on $Pt_{80}Fe_{20}$ (a) and modified $Pt_{80}Fe_{20}$ (b). In order to determine the charge-density difference upon adsorption of a molecule we calculate the total charge density and subtract the charge distribution obtained from calculations of the molecule and the surface alone. The latter calculations are carried out in the geometries of the relaxed adsorbate/substrate system, using the same supercell and number of grid points for numerical evaluation of the charge density. The shaded areas in Fig. 8 display an isosurface of the charge density difference, corresponding to the same numerical value of charge gain and loss in both subfigures. Dark and light shading represent positive and negative charge flow, respectively. The oxygen–metal bond is highlighted.

In the left subfigure the most prominent features come from the diσ_{CC} interaction, more specifically from the back-donation of surface charge to the prenal molecule along the Pt–C bonds. The Pt–O interaction is much weaker, and hardly represented by the chosen isosurfaces. Switching to panel b the situation changes completely. The surface iron atom looses a considerable amount of charge in a region pointing toward the oxygen atom, but both partners of the bond become polarized, so that the total charge in a sphere around the atoms changes only by 0.1 electrons. The charge redistribution extends over all of the adsorbate, influencing all of its atoms as far as the hydrogen atoms of the terminate methyl groups. The charge flow due to the diσ interaction of the C=C double bond is hardly discernible any more. The result corroborates that the bonding arrangements in the conjugated π-system change significantly. The C1=O and C2=C3 bonds loose some of their double bond character and become destabilized, while the C1–C2 bond gains electrons, which was already suggested by the respective changes in the bond lengths (cf. Table 3). This might have considerable implications for the activation of both double bonds to hydrogenation.

6. Vibrational frequencies

Vibrational spectra are a powerful means of investigating adsorption structures experimentally and to compare them to theoretical results. de Jesús and Zaera [31] have discussed the reflection-adsorption infrared spectra for multilayer coverages of acrolein and crotonaldehyde on Pt (111). They successfully identified the C–C single- and double-bond stretching frequencies as well as the C=O stretching frequency and several C–H vibrations. As we will show below these characteristic frequencies are highly dependent on the substrate and the adsorption geometry, which allows determination of the prevalent adsorption mode from the knowledge of the vibrational spectrum.

In Section 2 we have outlined our method to calculate vibrational spectra. The surface atoms were kept fixed when approximating the force-constant matrix, a simplification justified by the large mass difference between adsorbate and surface atoms. In Table 4 we demonstrate the accuracy of this method by comparing experimental and calculated values for the vibrational frequencies of gaseous acrolein (2-propenal). The agreement is remarkable. The calculated frequencies deviate less than 3% from the experimental ones, except for the lowest frequency, which is 36% off.

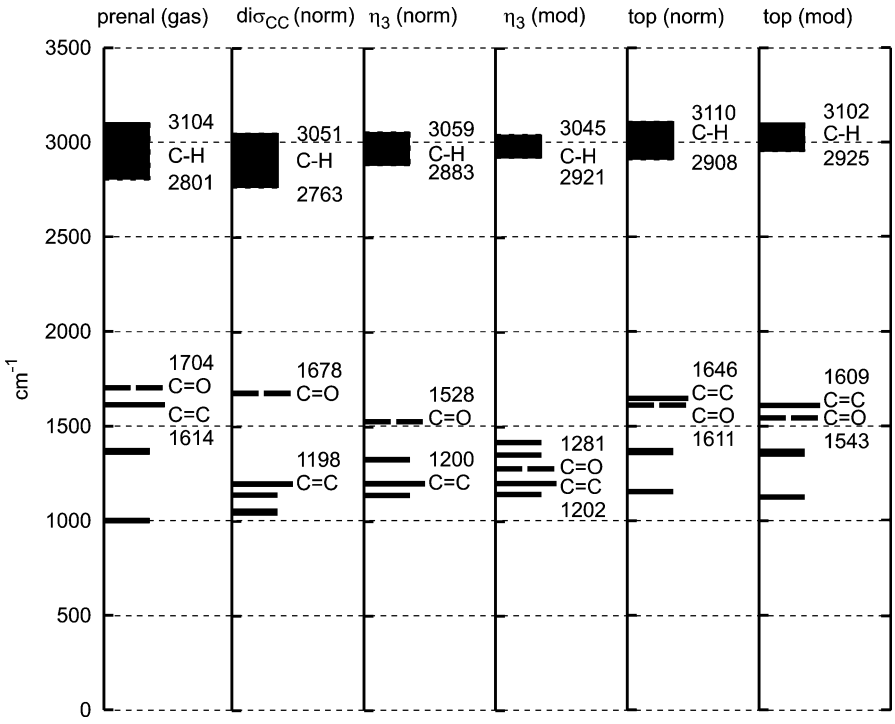

Fig. 9. Vibrational spectra of prenal in the gas phase and adsorbed on platinum-covered (norm) and modified (mod) $Pt_{80}Fe_{20}$ in different adsorption geometries. The eight C–H stretching frequencies are combined in a single C–H block. C=C and C=O frequencies are labeled, other lines correspond to (more or less pronounced) C–C frequencies.

Table 4
Experimental (cf. Ref. [45]) and calculated vibrational frequencies for gaseous acrolein (2-propenal) (a and s denoting asymmetric and symmetric stretchings, ip and op standing for in-plane and out-of-plane, respectively)

Type	Experiment (cm^{-1})	Theory (cm^{-1})	Type	Experiment (cm^{-1})	Theory (cm^{-1})
CH_2 a-str.	3103	3168	C–C str.	1158	1159
C2H str.	3028	3133	C2H op-bend	993	1016
CH_2 s-str.	3000	3064	C1H op-bend	980	1001
C1H str.	2800	2820	CH_2 wag	959	984
CO str.	1724	1700	CH_2 rock	912	931
C=C str.	1625	1626	CH_2 twist	593	610
CH_2 scis.	1420	1424	CCO deform	564	557
C1H ip-bend	1360	1353	CCC bend	327	328
C2H ip-bend	1275	1273	C–C torsion	157	214

The exact determination of the whole eigenvalue spectrum of a matrix, whose highest and lowest eigenvalue differ by a factor of 20, requires extremely precise calculations of energy differences and forces. For a typical displacement of 0.02 Å of a single atom from the ground-state configuration the changes in energy and forces are as low as 0.5 meV and 0.05 eV/Å, respectively. The three stretching frequencies of the molecule's frame (O=C1, C1–C2, C2=C3), including the two double-bond vibrations, are on average accurate within 1%. C–H bond frequencies are consistently too large, an error due to the neglect of either quantum effects or anharmonicity. Note that also the ordering of all frequencies agrees between theory and experiment.

Having proven the reliability of calculated vibrational frequencies we can now investigate the frequency shifts upon adsorption. In Fig. 9 we have collected the main frequencies of prenal in the gas phase as well as adsorbed on platinum-covered and modified $Pt_{80}Fe_{20}$ alloy surfaces in different adsorption geometries. It must be noted at this point, however, that we did not yet take intensities into account. In principle this is possible through the determination of the changing dipole moment upon vibration [48] but it is very demanding in terms of CPU time, on one hand, because of the larger vacuum needed and, on the other hand, because of the slower convergence of the wavefunctions upon self-consistent determination of the system's dipole moment. The eight C–H stretching frequencies are combined into a single C–H block, whose upper and lower bounds is given. The stretching frequencies of the two double bonds are labeled. These vibrations remain well separated regardless of the adsorption configuration. The C–C vibrations on the other hand become rather obscured and mixed with other modes.

Two very prominent features are observable: (a) Stretching frequencies of double bonds interacting with the surface become shifted toward lower values proportional to the interaction strength, while in each case the other double bond is only marginally influenced. (b) The C–H block becomes narrower as the oxygen atom interacts more strongly with the surface; particularly the lower bound of the block is shifted upward in wavenumber. The lowest C–H vibration is always C1–H. As the oxygen–carbon double bond weakens and oxygen looses influence in the bond, the stretching

frequency approaches the value of other C–H stretching vibrations.

A diσ_{CC} interaction with the surface results in a downshift of the C=C stretching frequency by about 400 cm^{-1}, independent of other adsorbate-surface interactions or the details of the surface-layer composition. The frequency shift of the C=O bond stretching depends on the oxygen-metal interaction. The difference of 250 cm^{-1} (η_3-adsorption) or 80 cm^{-1} (top adsorption), depending on whether iron is present in the surface or not, should be discernible in experimentally obtained vibrational spectra. However, being more or less horizontal vibrations in the η_3-mode, they might not be connected with a considerable change in the dipole moment normal to the surface, complicating experimental identification. Respective HREELS measurements are currently being performed (Y. Jugnet, private communications). They will be discussed and compared to our calculations in a forthcoming publication.

7. Conclusions

Starting from the adsorption of the α,β-unsaturated aldehydes acrolein and prenal on pure Pt (111) surfaces published recently [13], the influence of alloying platinum with 20 at% of Fe has been investigated. From previous experiments [31] it was concluded that acrolein adsorbs in a flat configuration on Pt (111) with both double bonds interacting with the surface, in agreement with theoretical results. Assuming an η_4 adsorption it is initially unclear which bond becomes hydrogenated. The experiments cited above suggest that the main reaction of acrolein is the decarbonylation to carbon monoxide and ethylene. The main theoretical result, however, is that hydrogenation toward an unsaturated alcohol is unlikely, as expressed by the comparatively low adsorption energy in configurations where only the C=O bond interacts with the surface.

When alloying Pt with Fe, a strong segregation of Pt toward the clean surface is observed. The initial model therefore contains a pure platinum surface layer. Compared to a pure Pt (111) crystal all adsorption energies are reduced, however, with no considerable change of relative stabilities of different adsorption modes. The underlying electronic structure changes have been discussed elsewhere [12]. When iron atoms are present in the surface, adsorption geometries including O–Fe interactions become by far the most stable ones. The adsorption energies are strongly increased, becoming even larger than on pure Pt (111). Still the most stable geometries are flat configurations with *both* double bonds interacting with the surface. Experimental investigations of Birchem et al. [46] have suggested a second (vertical) adsorption mode for high coverages of prenal on pure Pt (111). While such a top adsorption might be competitive also in the framework of DFT calculations on the pure Pt surface [13], this is not the case on the alloy, even with iron present in the surface. Taking into account dipole corrections to rectify errors introduced by the periodic calculational setup and considering entropy terms at finite temperatures, a possible vertical adsorption of prenal seems to be replaced by a flat adsorption geometry already at temperatures well below catalytic conditions (room temperature).

The huge adsorption-energy gain upon adsorption including Fe–O bonds can lead to a substantial change in the segregation profile as a simple quasi-chemical model has shown, rising the iron concentration in the surface. Such adsorption-induced changes of the segregation profile have also experimentally been identified at 323 K without further thermal treatment of the surface [42]. We additionally want to point out that the LEED model of the $Pt_{80}Fe_{20}$ surface allows for a low percentage of Fe in the surface layer [27], which has previously been quoted by experimentalists to explain temperature-programmed desorption (TPD) peaks of atomic hydrogen on this surface [47]. The conclusion that iron atoms in the surface are needed for a selective hydrogenation of unsaturated aldehydes toward unsaturated alcohols is corroborated by experimental results (cf. Table 1). In $Pt_{0.8}Fe_{0.2}$ particles where the probability to find Fe atoms in the surface is higher than in well-prepared $Pt_{80}Fe_{20}$ (111) surfaces, the selectivity is more pronounced.

The influence of iron atoms in the surface on the electronic structure was discussed. A charge transfer from the electropositive iron atom to the adsorbate's oxygen atom is connected with an activation of the entire adsorbate molecule. The platinum-oxygen interaction in the case of a platinum-covered surface is only faintly observable. Finally, we discussed vibrational spectra as a means to connect our results to experiments.

Adsorption of α,β-unsaturated aldehydes on $Pt_{80}Fe_{20}$ includes very strong Fe–O bonds, weakening the C=O double bond. This, however, does not conclusively explain the selective hydrogenation of unsaturated aldehydes toward unsaturated alcohols. A flat adsorption configuration including the interaction of both double bonds with the surface is also energetically favored on the pure Pt (111) surface. However, a substantially weakened C=O double bond which is found only when Fe atoms are present in the surface is certainly more likely to be hydrogenated than the same but much stronger bond in a molecule adsorbed on a pure Pt surface layer. Furthermore, the higher selectivity for prenal (having two methyl groups at the C3 atom) compared to acrolein, the most simple of the α,β-unsaturated aldehydes, can be understood considering the reduced interaction of the C=C bond with the surface.

Still, two questions remain, that can at this point be answered only speculatively: Why does the hydrogenation start with the C=O double bond on the alloy surface while the main catalytic product over the pure Pt surface (at least for small aldehydes) is the saturated aldehyde? For prenal over Pt (111) most often both double bonds are hydrogenated, leading to the saturated alcohol (cf. Table 1), why does the reaction stop after the first hydrogenation step on the alloy surface? The first question is partly answered by

the weakening of the C=O bond through Fe–O interactions. Furthermore there might be an additional cooperative effect with coadsorbed hydrogen atoms that preferably approach the C=O double bond. The second question might be answered by the low adsorption energy of the diσ_{CC} mode on the alloy surface. The adsorbate after the hydrogenation of the C=O double bond, the unsaturated alcohol, will most likely only adsorb in a diσ mode. Two effects can contribute to the desorption of the molecule rather than further hydrogenation to the saturated alcohol. On one hand, it is known from previous studies on the hydrogenation of ethylene over Pt (111) surfaces that the energy barrier for the hydrogenation of a C=C double bond is around 0.8 eV [49]. The reaction barrier for the hydrogenation of the C=C double bond is therefore higher than the adsorption energy of the unsaturated alcohol on the alloy. On the other hand the adsorption of the unsaturated aldehyde in the η_3-*cis* or η_4-*trans* configuration is very stable. Hence, even without the attempt to hydrogenate the C=C double bond in the unsaturated alcohol, it might desorb by competition with the unsaturated aldehyde as long as this reactant is not completely converted. A forthcoming article will deal with these issues in detail.

Acknowledgments

We gratefully acknowledge financial support by the European Commission's Human Potential Programme (Marie Curie Training Site No. MCFH-1999-01219) and the Austrian Fonds zur Förderung der Wissenschaftlichen Forschung within the Science College "Computational Materials Science" (FWF-WK004). Furthermore we thank the CINES and IDRIS (project 609) Computer Centers in Montpellier and Orsay respectively for generous provision of CPU time. Vibrational spectrum calculations were performed on the Schrödinger I cluster at the Vienna University Computer Center. The authors thank Yvette Jugnet for fruitful discussions.

References

[1] P. Claus, Topics Catal. 5 (1998) 51.
[2] V. Ponec, Appl. Catal. A 149 (1997) 27.
[3] P. Gallezot, D. Richard, Catal. Rev. Sci. Eng. 40 (1998) 81.
[4] M.A. Vannice, B. Sen, J. Catal. 115 (1989) 65.
[5] C. Mohr, P. Claus, Sci. Progr. 84 (2001) 311.
[6] P. Beccat, J.C. Bertolini, Y. Gauthier, J. Massardier, P. Ruiz, J. Catal. 126 (1990) 451.
[7] M. English, V.S. Ranade, J.A. Lercher, J. Mol. Catal. A 121 (1997) 69.
[8] T.B.L.W. Marinelli, S. Nabuurs, V. Ponec, J. Catal. 151 (1995) 431.
[9] N. Homs, J. Llorca, P. Ramírez de la Piscina, F. Rodríguez-Reinoso, A. Sepúlveda-Escribano, J. Silvestre-Albero, Phys. Chem. Chem. Phys. 3 (2001) 1782.
[10] W. Kohn, L.J. Sham, Phys. Rev. 140 (1965) A1133.
[11] U. von Barth, L. Hedin, J. Phys. C 5 (1972) 2064.
[12] R. Hirschl, F. Delbecq, P. Sautet, J. Hafner, Phys. Rev. B 66 (2002) 155438.
[13] F. Delbecq, P. Sautet, J. Catal. 211 (2002) 398.
[14] G. Kresse, J. Furthmüller, Phys. Rev. B 54 (1996) 11169.
[15] G. Kresse, J. Hafner, Phys. Rev. B 47 (1993) 558.
[16] J.P. Perdew, Y. Wang, Phys. Rev. B 45 (1992) 13244.
[17] H.J. Monkhorst, J.D. Pack, Phys. Rev. B 13 (1976) 5188.
[18] P.E. Blöchl, Phys. Rev. B 50 (1994) 17953.
[19] G. Kresse, D. Joubert, Phys. Rev. B 59 (1999) 1758.
[20] G. Makov, M.C. Payne, Phys. Rev. B 51 (1994) 4014.
[21] J. Neugebauer, M. Scheffler, Phys. Rev. B 46 (1992) 16067.
[22] R.P. Feynman, Phys. Rev. 56 (1939) 340.
[23] M. Polak, L. Rubinovich, Surf. Sci. Rep. 38 (2000) 127.
[24] C. Creemers, Surf. Sci. 360 (1996) 10.
[25] C. Creemers, P. Deurinck, Surf. Interface Anal. 25 (1997) 177.
[26] C. Creemers, H. van Hove, A. Neyens, Appl. Surf. Sci. 7 (1981) 402.
[27] P. Beccat, Y. Gauthier, R. Baudoing-Savois, J.C. Bertolini, Surf. Sci. 238 (1990) 105.
[28] N. Barrett, C. Guillot, J.C. Bertolini, J. Massardier, B.C. Khanra, Surf. Sci. Lett. 260 (1992) L11.
[29] R.M. Watwe, R.D. Cortright, M. Mavrikakis, J.K. Nørskov, J.A. Dumesic, J. Chem. Phys. 114 (2001) 4663.
[30] J. Silvestre-Albero, M.A. Sanchez-Castillo, R. He, A. Sepúlveda-Escribano, F. Rodríguez-Reinoso, J.A. Dumesic, Catal. Lett. 74 (2001) 17.
[31] J.C. de Jesús, F. Zaera, Surf. Sci. 430 (1999) 99.
[32] J.E. Bailie, C.H. Rochester, G.J. Hutchings, J. Chem. Soc. Faraday Trans. 93 (1997) 4389.
[33] P. Claus, A. Brückner, C. Mohr, H. Hofmeister, J. Am. Chem. Soc. 122 (2000) 11430.
[34] F. Delbecq, P. Sautet, Langmuir 9 (1993) 197.
[35] A. Grassi, P. Longo, A. Musco, W. Porzio, A. Srivanti, J. Organomet. Chem. 289 (1985) 439.
[36] G. Wu, Y. Zhang, L. Ribaud, P. Coppens, C. Wilson, B.B. Iversen, F.K. Larsen, Inorg. Chem. 37 (1998) 6078.
[37] J.L. Rousset, J.C. Bertolini, P. Miegge, Phys. Rev. B 53 (1996) 4947.
[38] A.D. Sarkar, B.C. Khanra, Phys. B 315 (2002) 82.
[39] M. Menon, B.C. Khanra, Int. J. Mod. Phys. 14 (2000) 1683.
[40] S. Deckers, F.H.P.M. Habraken, W.F. van der Weg, A.W.D. van der Gon, B. Pluis, J.F. van der Veen, R. Baudoing, Phys. Rev. B 42 (1990) 3253.
[41] S. Deckers, F.H.P.M. Habraken, W.F. van der Weg, A.W.D. van der Gon, J.F. van der Veen, J.W. Geus, Appl. Surf. Sci. 45 (1990) 121.
[42] C.J. Baddeley, L.H. Bloxham, S.C. Laroze, R. Raval, T.C.Q. Noakes, P. Bailey, J. Phys. Chem. B (2001).
[43] F. Delbecq, P. Sautet, J. Catal. 164 (1996) 152.
[44] B. Hammer, J.K. Nørskov, Nature (London) 376 (1995) 238; Adv. Catal. 45 (2000) 71.
[45] T. Simanouchi, Tables of Molecular Vibrational Frequencies Consolidated, Volume I, National Bureau of Standards, Gaithersburg, MD, 1972.
[46] T. Birchem, C.M. Pradier, Y. Berthier, G. Cordier, J. Catal. 146 (1994) 503.
[47] A. Atli, M. Almot, J.J. Ehrhardt, J.C. Bertolini, M. Abon, Surf. Sci. 269 (1992) 365.
[48] A. Eichler, Surf. Sci. 526 (2003) 332.
[49] M. Neurock, V. Pallassana, R.A. van Santen, J. Am. Chem. Soc. 122 (2000) 1150.